32nd International Cosmic Ray Conference, Beijing 2011

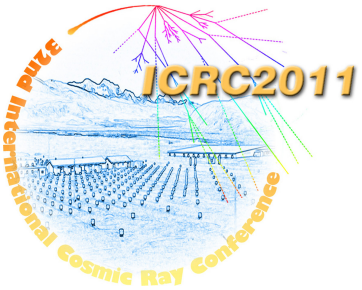

CREAM: Results, Implications and Outlook

E. S. Seo on behalf of CREAM collaboration[1,2;1)]

[1] Institute for Physical Science and Technology, University of Maryland, College Park, MD 20742, USA
[2] Department of Physics, University of Maryland, College Park, MD 20742, USA

Abstract: The Cosmic Ray Energetics And Mass (CREAM) balloon-borne experiment has accumulated ∼161 days of exposure during six successful flights over Antarctica. Energy measurements are made with a transition radiation detector and an ionization calorimeter. Charge measurements are made with timing scintillators, pixelated Si, and Cherenkov detectors to minimize the effect of backscattered particles. High energy cosmic-ray data were collected over a wide energy range from $\sim 10^{10}$ to $\sim 10^{15}$ eV at an average altitude of ~ 38.5 km, with ~ 3.9 g/cm^2 atmospheric overburden. All cosmic-ray elements from protons ($Z=1$) to iron nuclei ($Z=26$) are separated with excellent charge resolution. Recent results from the ongoing analysis including the discrepant hardening of elemental spectra at ~ 200 GeV/n are presented and their implications on cosmic-ray origin, acceleration and propagation are discussed. The project status and plans are also presented.

Key words: elemental spectra, balloon flights, CREAM

1 Introduction

The Cosmic Ray Energetics And Mass (CREAM) instrument was designed and constructed to measure cosmic ray elemental spectra to the highest energy possible with a series of Ultra Long Duration Balloon (ULDB) flights [1]. The goal was to understand the origin, acceleration and galactic propagation of the bulk of cosmic rays. This included whether and how the "knee" structure in the all-particle spectrum observed by air shower experiments is related to the mechanisms of acceleration, propagation, and confinement. The instrument was designed to meet the challenging and conflicting requirements to have a large enough geometry factor to collect adequate statistics for the low flux of high energy particles, and yet stay within the weight limit for balloon flights. It has redundant and complementary charge identification and energy measurement systems capable of direct measurements of elemental spectra for $Z=1-26$ nuclei over the energy range $\sim 10^{10}-10^{15}$ eV.

The ULDB vehicle is still not proven, but six CREAM payloads have flown successfully on conventional zero pressure balloons [2]. The 40 million cubic foot (MCF) balloon can carry a total suspended weight of 6,000 lb, which allows a large amount (∼1,200 lb) of ballast for the ∼2,500 lb CREAM instrument. The balloons were launched from McMurdo, Antarctica, and with one exception each flight subsequently circumnavigated the South Pole two or three times. The launch and termination dates and the flight duration for each flight are summarized in Table 1. A 40 MCF-lite conventional balloon carried each payload to its float altitude between ∼38 and ∼40 km. The balloon kept a stable altitude

Table 1. Summary of the six CREAM balloon flights in Ant-arctica

	Launch	Termination	Duration
CREAM-I	2004.12.16	2005.1.27	42 days
CREAM-II	2005.12.15	2006.1.13	28 days
CREAM-III	2007.12.19	2008.1.17	29 days
CREAM-IV	2008.12.18	2009.1.7	19 days
CREAM-V	2009.12.1	2010.1.8	37 days
CREAM-VI	2010.12.21	2010.12.26	6 days

1) E-mail: seo@umd.edu

DOI: 10.7529/ICRC2011/V12/H16

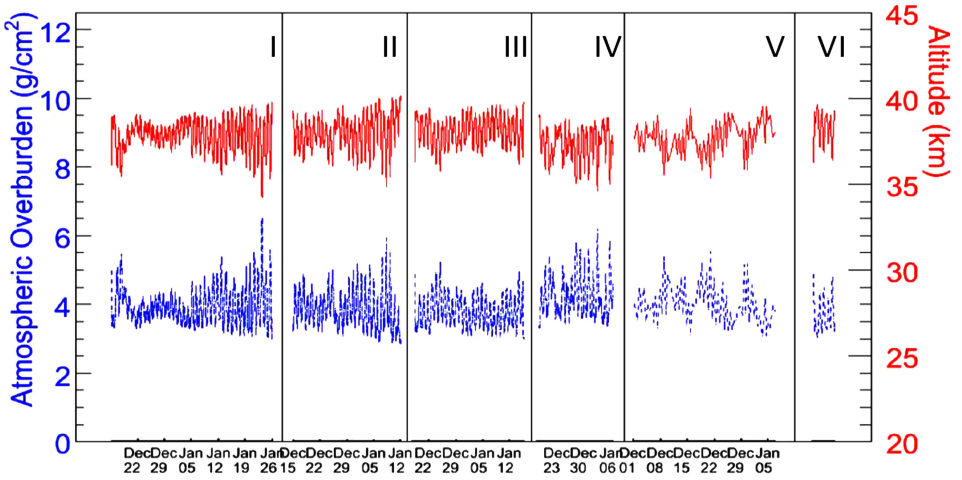

Fig. 1. Altitude of the balloon (upper solid lines) and the corresponding atmospheric overburden in g/cm2 (lower dashed lines) as a function of time for six CREAM flights.

profile with a corresponding average atmospheric overburden of ~ 3.9 g/cm^2 for all 6 flights as shown in Figure 1. The small diurnal variation is due to Sun angle changes. CREAM has accumulated ~ 161 days of flight data, the longest known exposure for a single balloon project.

2 The CREAM Instrument

In contrast to most balloon payloads, the CREAM science instrument is not pressurized, in order to be more robust for ULDB flights. The CREAM-I to -IV instruments were supported with the Command and Data Handling Module (CDM) developed by the NASA Wallops Flight Facility for ULDB flights. The CDM is nearing the end of its useful lifetime without a spare. To mitigate the risk of damaging or losing the CDM, the CREAM data acquisition system (DAQ) was modified to accommodate the Support Instrumentation Package (SIP) normally used by the Columbia Scientific Balloon Facility (CSBF) to support Long Duration Balloon (LDB) payloads. The main difference between the CDM and SIP from the instrument interface viewpoint is that the SIP is serial-based, whereas the CDM is ethernet-based. The modified CREAM DAQ with the serial interface was successfully used in both CREAM-V and CREAM-VI. The payload has been recovered successfully after each flight, refurbished, and calibrated at the European Organization for Nuclear Research (CERN) for the next flight.

The science instrument consists of complementary and redundant particle detectors to determine the charge and energy of high-energy particles [3]. The instrument configuration for CREAM-VII is shown in Figure 2. The highly segmented detectors comprising the instrument have $> 10,000$ electronic channels. They include a large Silicon Charge Detector (SCD-L), Timing Charge Detector (TCD), Transition Radiation Detector (TRD), Cherenkov Detector (CD), double layer Silicon Charge Detector (SCD), carbon targets, and an ionization calorimeter comprised of a stack of tungsten plates with interleaved scintillating fiber layers. All detectors have been flown at least

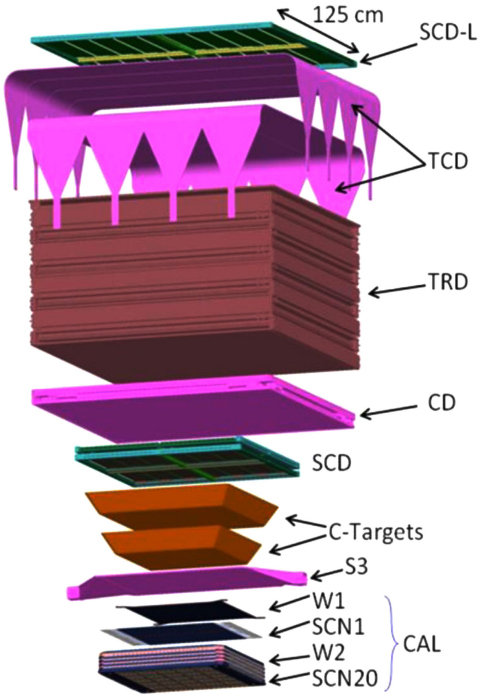

Fig. 2. Schematic of the CREAM-VII instrument configuration.

twice, except for the newly constructed TRD, which incorporates improvements in the CREAM-I TRD technology, and SCD-L which is a larger area version of the SCD.

For CREAM-III to -VI, the Cherenkov Camera (CherCam) replaced the TRD. The suspended weight of CREAM-III was 2,670 kg, including the $\sim 1,000$ kg instrument and ~ 545 kg of ballast. The power consumption of the instrument was ~ 480 W, higher than the previous flight but well within the power budget.

The TCD defines a trigger aperture of 2.2 m^{2}sr and measures the incident particle charge using fast electronics before backscattered particles hit the detector. The CD with a 1 cm thick wavelength-shifted Cherenkov radiator vetoes low-energy background particles due to the low geomagnetic cutoff over Antarctica. A single layer of 2×2 mm^2 square scintillating fibers, S3, measures the time at which backscattered particles start their way back to the TCD. The TRD determines the Lorentz factor of $Z \geq 3$ nuclei by measuring transition X-rays using thin-wall gas tubes. The SCD is segmented into small pixels (2.12 cm^2) to minimize hits of accompanying backscattered particles in the same segment as the incident particle. The calorimeter combines 0.5 $\lambda_{\rm int}$ thick graphite targets and a stack of 20 tungsten plates, each 50 cm $\times$ 50 cm $\times$ 3.5 mm (1 X_0) thick, followed by a layer of 0.5 mm diameter scintillating fibers grouped into fifty 1 cm-wide ribbons. The carbon target induces hadronic interactions so showers develop in the calorimeter. Energy deposition in the calorimeter determines the particle energy and provides tracking information to determine which segment(s) of the charge detectors to use for the charge measurement. Tracking for showers is accomplished by extrapolating each shower axis back to the charge detectors. Tracking for non-interacting particles in the TRD is achieved with better accuracy (1 mm resolution with 67 cm lever arm, 0.0015 radians). The TRD and calorimeter, which can also measure the energy of protons and He, have different systematic biases in determining particle energy. The use of both instruments allows in-flight cross-calibration of the two techniques for $Z > 3$ particles, which leads to a powerful method for measuring cosmic-ray energies [4]. They can also be used to distinguish electrons from protons, thereby enabling CREAM measurement of the rare high-energy electrons, which is currently a topic of great scientific interest [5,6].

Details about the performance of instruments flown on previous flights can be found elsewhere: Calorimeter [7,8]; CherCam [9]; TRD/TCD [10,11]; and SCD [12,13]. Newly developed detectors, SCD-L and TRD, are described below.

2.1 SCD and SCD-L

The SCD is comprised of an array of DC-type silicon PIN diodes. A cosmic ray passing through the sensor produces ionization in the depleted region that is proportional to the square of the particle charge. The building block of the SCD is a silicon sensor fabricated on a 5 inch, 380 μm thick wafer. The sensor is segmented into a 4×4 matrix of 16 pixels. The 2.12 cm^2 active area of each pixel is optimized to reduce the effect of backscatter from showers in the calorimeter, while keeping the channel count and power at manageable levels. The readout electronics are designed around a 16-channel CR-1.4A ASIC for each sensor followed by 16 bit ADC's. This allows fine charge resolution over a wide dynamic range covering up to $Z = 33$ signals. A single layer SCD consists of 26 ladders, each holding seven silicon sensor modules with associated analog readout electronics to cover 79×79 cm^2 area.

Individual elements are clearly identified in the SCD with charge resolution better than 0.2e for protons and helium, 0.2e for oxygen, and slightly worse than 0.2e for higher charges. An improvement for CREAM-II and subsequent flights over CREAM-I was a dual-layer SCD, which consists of a total of 4,992 pixels. Excellent charge resolution was obtained by requiring consistency between the two charge measurements. The charge peaks for each element from $Z = 1$ to 28 are clearly separated as shown in Figure 3. The relative abundance in this plot has no physical

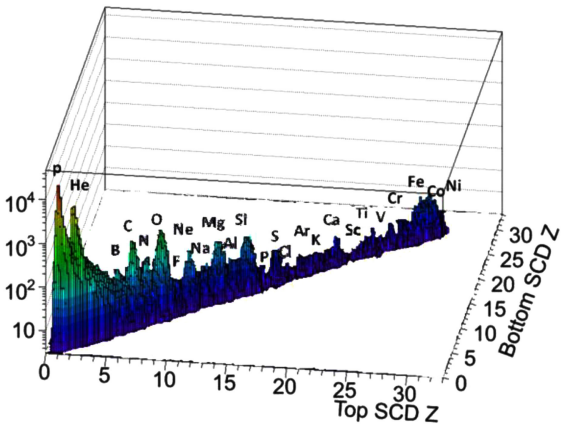

Fig. 3. Distribution of cosmic-ray charge measured with the dual layer SCD. The charge reconstructed for a fraction of the flight data is shown in units of elementary charge e.

significance, because needed corrections for interactions and propagations have not been applied to these data.

The same SCD was flown repeatedly for the last 5 flights. The total fraction of dead and noisy channels (1.7% for CREAM-III) increased with time to about 7% for CREAM-VI. Considering this aging effect, a duplicate of the SCD was developed. In addition, a large silicon charge detector (SCD-L) was developed to place at the top of the CREAM-VII instrument (see Figure 2). Like the SCD, the detector unit is a DC-type silicon PIN diode sensor, but it was fabricated on a 6 inch, 525 μm thick wafer. A sensor is comprised of 16 pixels arranged in a 4 by 4 matrix, having dimensions of 5.8×6.3 cm^2. Each pixel would be larger than that of the SCD but the total number of channels would be similar to the double layer SCD. The sensitive area of SCD-L is 120×120 cm^2, and its overall height is ~ 10 cm. The mass and power consumption are estimated to be 80 kg and 150 Watts, respectively.

SCD-L will measure the charge of incident nuclei before they interact in the material of the lower detectors. Secondary particles from charge changing interactions above the SCD (e.g., in the TRD or CherCam) could be removed by requiring consistency between the two charge measurements. This would improve our current estimates on secondary corrections based on Monte Carlo simulations. A combination of the double layer SCD and single layer SCD-L with a long lever arm allows precise trajectory determination of passing-through particles.

2.2 TRD

The new TRD consists of two sections, each with 4 modules. Each module is comprised of a 50 mm thick Styrofoam (32 kg/m^3 density) radiator and 200 straw tubes in double layers with alternating orthogonal straw orientations. The straw tubes are made of thin aluminized Mylar and filled with a Xe/CO_2 80%/20% gas mixture. The straws were tested at 3 bar overpressure for the weld quality and gas diffusion rate, required to be less than 0.01 mbar/min at 1 bar. The TRD utilizes 10 mm diameter straw tubes to improve particle tracking over the CREAM-I 20 mm tube design, thereby enhancing charge identification in the SCD. The tracking accuracy improvement will also reduce uncertainties of path-length corrections for the TRD and other CREAM sub-detector signals.

The signals from straw tubes are read out by VA32HDR11 front-end ASIC chips. The front-end readout electronics contain a low-power FPGA-based sequencer, driven by the CREAM Master Trigger (CMT), to control the ASIC sample and hold, the analog multiplexer, serial ADC and clear logic. The front-end performs data sparsification (zero-suppression) and sends significant data to the main DAQ board. It provides a good signal-to-noise ratio per channel, low cross-talk and coherent noise levels, and a large dynamic range to measure energy for $3 < Z < 26$ nuclei in the Lorentz factor range of 10^2–10^5. Compact new electronics replaced the bulky VME based electronics box of the CREAM-I TRD.

The TRD was calibrated at the CERN SPS H2B in 2010 with various momentum hadron and electron beams. The beam calibration was done together with the CREAM calorimeter and SCD. They have been tested in thermal vacuum to find no HV discharges, gas leaks or manifold temperature surges. Due to the deformation of Ethafoam-220, our initial choice, the radiator material was changed to Styrofoam. More details of the TRD design and various test results are reported in another paper [14]. The assembled TRD is shown in Figure 4. Long term qualification tests, including gas leak rate test at high pressure and readout system test on cosmic muons, will continue until the CREAM-VII launch.

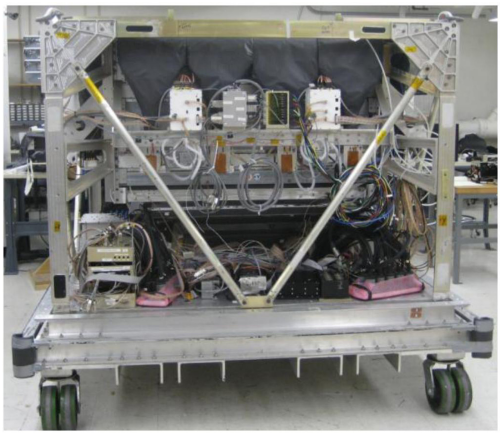

Fig. 4. A photo of CREAM-VII during the integration with the TCD, a new TRD, and the calorimeter module recovered from CREAM-VI.

3 Current results and implications

As described in [15,16], for events selected with the high energy (calorimeter) trigger, the shower axis is reconstructed by a linear fit of the scintillating fiber strip with the maximum energy deposit in each layer. This reconstructed trajectory is required to traverse the SCD active area and the bottom of the calorimeter active area. The particle energy is determined

from energy deposit in the calorimeter. All-particle counts are shown as a function of incident energy in Figure 5. This plot is not intended for spectral index or absolute flux measurements, but rather for a quick consistency check. It does not include the energy dependent shower leakage corrections for the energy scale, and no corrections have been made for charge dependent efficiencies. Due to improved readout electronics [7], the CREAM-III to -VI data indicate an energy threshold significantly lower than in the first two flights. The six flight-data sets follow a consistent power law above the calorimeter threshold (low energy roll off), and they cover 3 decades in energy.

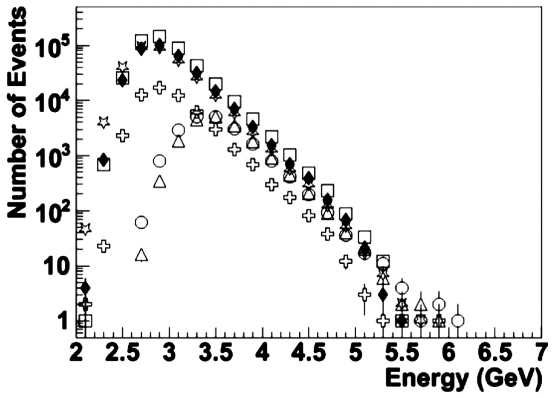

Fig. 5. All-particle counts as a function of incident energy for the previous 6 flights are compared: CREAM-I (circles), CREAM-II (triangles), CREAM-III (squares), CREAM-IV (stars), CREAM-V (diamonds) and CREAM-VI (crosses).

3.1 Discrepant hardening of Spectra

One of the key results from the ongoing analysis of CREAM data is that proton and helium spectra are not the same: power-law fits (flux $\sim E^{\gamma}$) yield indices γ of -2.66 ± 0.02 for protons and -2.58 ± 0.02 for helium, respectively. Our helium fluxes are 4 standard deviations higher than would be indicated by extrapolation of a single power-law fit of the low energy helium data, e.g., Alpha Magnet Spectrometer - AMS, to our measurement energies. Our proton-to-helium ratio, 8.9 ± 0.3 at ~ 9 TeV/nucleon, is significantly lower than the AMS ratio $\sim 18.8 \pm 0.5$ at 100 GeV/nucleon [16]. An explanation could be that protons and helium come from different types of sources or acceleration sites. The difference between protons and helium has been a tantalizing question, because spectral indices determined from measurements over the limited energy range of a single experiment could not provide a definitive answer.

The Payload for Antimatter Matter Exploration and Light Nuclei Astrophysics (PAMELA) space mission uses a permanent magnet spectrometer with a variety of detectors for precision measurements of the abundance and energy spectra of cosmic rays [17]. The energy reach of the high quality PAMELA data is very limited, but it measures electrons, positrons, antiprotons, and light nuclei over the energy range from 50 MeV to hundreds of GeV, depending on the species. As shown in Figure 6, PAMELA has recently reported direct observation of spectral hardening of proton and helium spectra around 200 GV, which was first seen in the CREAM data [18].

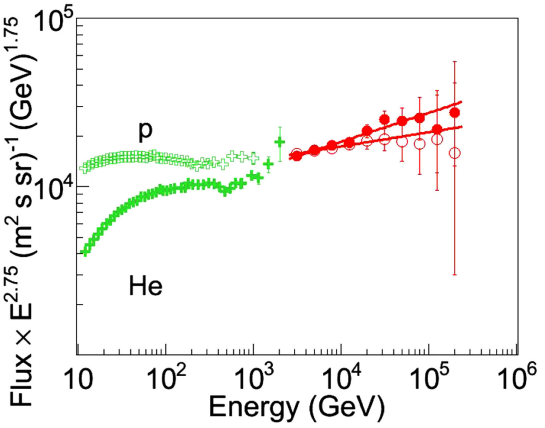

Fig. 6. Measured energy spectra of protons (open symbols) and helium nuclei (filled symbols): Green crosses for PAMELA and red circles for CREAM. The lines represent power-law fits to the CREAM data.

Spectral hardening is not limited to protons and helium. Heavier nuclei also show a harder spectrum for each element above ~ 200 GeV/nucleon, indicating departure from a single power law [18]. A broken power law fit for C, O, Ne, Mg, Si, and Fe with spectral indices γ_1 and γ_2, respectively, below and above 200 GeV/nucleon resulted in $\gamma_1 = -2.77 \pm 0.03$ and $\gamma_2 = -2.56 \pm 0.04$, which differ by 4.2σ. As shown in Figure 7, γ_1 is consistent with the low energy helium measurements, e.g., the AMS index of -2.74 ± 0.01, whereas γ_2 agrees remarkably well with the CREAM helium index of -2.58 ± 0.02 at higher energies. This spectral hardening above 200 GeV/n could imply that the source spectra are harder than previously thought based on the low energy data, or it could reflect the predicted concavity in the spectra before the "knee". In the framework of diffusive shock acceleration, cosmic-ray pressure created by particle interactions with the shock could broaden the shock

transition region, causing higher energy particles to gain energy faster. This could cause spectral flattening with increasing energy and deviations from a pure power law.

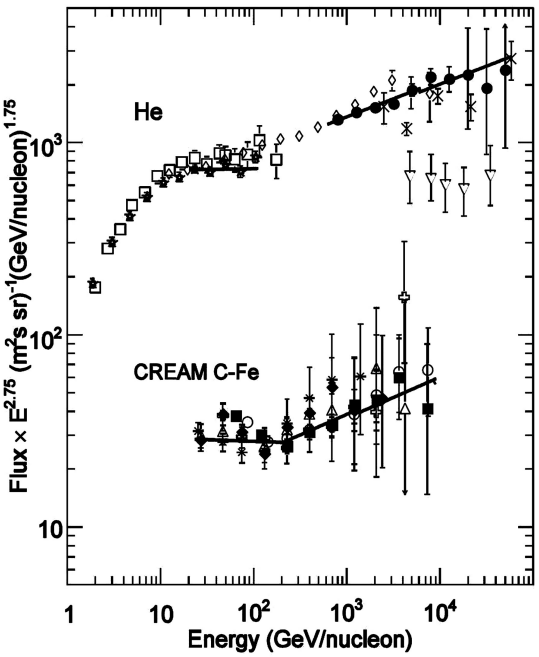

Fig. 7. Measured spectra of helium and heavier nuclei as a function of energy per nucleon (Ref. [18] and references therein). The lines for helium data re-present a power-law fit to AMS (open stars) and CREAM (filled circles), respectively. Also shown are helium data from other experiments: BESS (open squares), ATIC-2 (open diamonds), JACEE (X), and RUNJOB (open inverted triangles). The lines for C-Fe data represent a broken power-law fit to the CREAM heavy nuclei data: Carbon (open circles), Oxygen (filled squares), Neon (open crosses), Magnesium (open triangles), Silicon (filled diamonds), and Iron (asterisks). The broken power law fit for each element is normalized to the Carbon fit.

Alternatively, the observed hardening could be due to nearby sources, as suggested for the recent electron observations of ATIC [5], Fermi [6] and PAMELA [19]. The substantial contribution of a nearby and recent single source (SNR or pulsar) to the flux of protons and nuclei has been proposed to explain the "knee". A multi-source model in Ref. [20] considered novae stars and explosions in superbubbles as additional cosmic-ray sources. Whether it results from a nearby isolated SNR [21] or the effect of distributed acceleration by multiple remnants embedded in a turbulent stellar association [22] is another question.

Whatever the explanation, the CREAM results contradict the traditional view that a simple power law can represent cosmic rays without deviations below the "knee" around 3×10^{15} eV. The pervasive discrepant hardening in all of the observed elemental spectra provides important constraints on cosmic ray acceleration and propagation models, and it must be accounted for in explanations of the electron anomaly and mysterious cosmic ray "knee". As reported in Ref. [23] the spectral hardening would lead to appreciable modifications for the secondary yields, such as antiprotons and diffuse gamma rays, in the sub-TeV range. Using a simple power law to model the astrophysical background for indirect Dark Matter searches, as often done in the literature, might lead to wrong conclusions about the evidence of a signal. Or, if a signal should be detected, use of a power law could lead to bias in the inferred values of the parameters describing the new phenomena.

3.2 Propagation history

Cosmic rays reaching the earth result from a complex succession of physical processes starting with the primary seed population at the source, followed by ejection from the source and acceleration in supernovae shock waves. During their transport through the galactic magnetic field and interstellar gas/plasma, interactions with interstellar matter produce secondary cosmic-rays that reflect the amount of matter traversed. The cosmic rays propagate through the Galaxy by scattering off magnetic irregularities, described as diffusion. The propagation may be influenced by convection due to galactic wind and/or re-acceleration [24].

The rare elements, Li, Be, and B, in cosmic rays are believed to be produced as a result of fragmentation of heavier cosmic ray nuclei, e.g., C and O, in the interstellar medium (ISM). The relative abundance of these secondaries to primaries is a measure of the amount of material through which the cosmic rays pass before escaping the Galaxy. The measured B/C ratio of $0.2 - 0.3$ below 1 GeV/n corresponds to the average amount of material traversed by cosmic rays, $\lambda \sim 10$ g/cm^2. The ratio decreases as energy increases, i.e., λ decreases with energy, implying that high energy cosmic rays escape more readily than low energy ones. A typical form for the rigidity de-pendence of pathlength (in g/cm^2) is $\lambda = \lambda_0(R/R_0)^{-\delta}$, where λ is the mean escape pathlength, R is the nucleus magnetic rigidity, and δ is an

energy dependent parameter. The most commonly used and simplest propagation model is the Standard Leaky Box Model (SLBM) [25]. In this model, cosmic rays are confined in a volume ("box") where they undergo nuclear interaction with the ISM and produce secondaries, lose energy via ionization, or "leak out" with a small probability when they encounter the boundary of the box. Propagation in this model is described by the mean of the path length distribution.

The measured B/C ratios are compared with propagation models in Figure 8. The CREAM data [26] are consistent with the HEAO-3 [27] experiment at low energies, and ATIC [28] and TRACER [29] where they overlap. The curves represent three different δ values for the SLBM, as well as a reacceleration model [30]. The data indicate that the propagation pathlength of cosmic ray nuclei is smaller by an order of magnitude for particles in the TeV/n region compared to those at energies below 10 GeV/n. This high-energy path length (~ 1 g/cm^2) is still large compared to the typical grammage of the Galactic disk (≤ 0.002 g/cm^2).

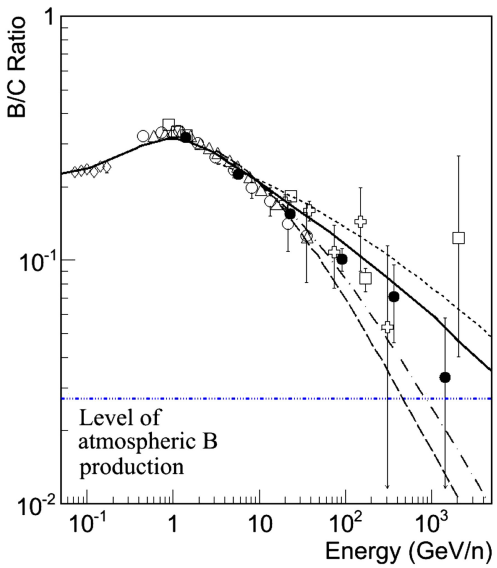

Fig. 8. Measured B/C ratio data and propagation models ([1] and references therein): CREAM-I (black circles), ATIC (open crosses), HEAO-3 (open triangles), TRACER (open squares), AMS-01 (open circles) and ACE (open diamonds). The curves represent power law mean pathlength with = 0.333, dotted line; = 0.6, dash-dot line; and =0.7, dashed line, for SLBM; and a solid line for a reacceleration model. A horizontal blue dash-dot line represents the level of atmospheric boron production.

Balloon-borne experiments have provided the highest energy B/C data and other relative abundances, but the statistical uncertainties are still too high to constrain propagation models. Future flight data from CREAM will reduce statistical uncertainties and extend the measurements to the energies where propagation models can be distinguished.

3.3 Source abundances

When comparing the galactic cosmic ray (GCR) source (GCRS) abundances with solar system (SS) abundances as a function of the first ionization potential (FIP), there is a general trend of lower GCR/SS with higher FIP [31].

Likewise, the same GCRS/SS ratios, as a function of elemental atomic mass, show a separation of refractory elements and volatile elements. The GCRS/SS ratio is generally higher for refractory elements than for volatile elements, as illustrated in Figure 9.

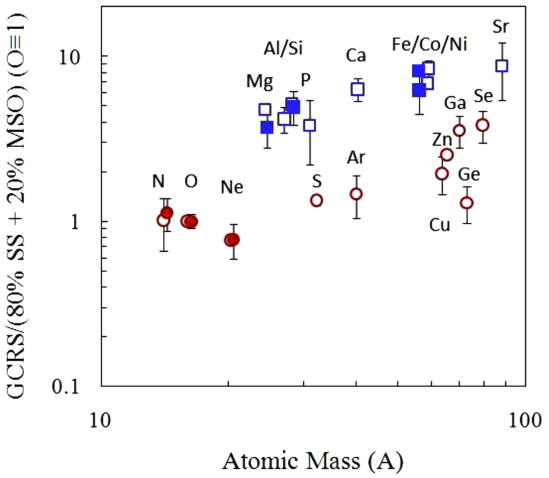

Fig. 9. Ratio of cosmic-ray source abundances to a mixture of 80% SS and 20% MSO as a function of atomic mass [1] and references therein. CREAM data (filled symbols) in the energy range from 500 GeV/n to ~ 4 TeV/n are compared to those of HEAO and TIGER data (open symbols) below 30 GeV/n. Refractory elements (blue squares) and volatile elements (red circles).

Using two Cherenkov counters with Aerogel and acrylic radiators and a pair of scintillating fiber hodoscopes sandwiched between two scintillators, Trans-Iron Galactic Element Recorder (TIGER) measured the elemental composition of the rare GCR heavier than iron, looking for clues to nucleosynthesis and the origin of cosmic rays. Rauch et al. [32]

reported that the data are best organized when the GCRS abundances are compared with SS including 20% Massive Star Outflow (MSO), and they follow two different power-law trends: $A^{2/3}$ for the refractory elements and A^1 for volatile elements. As shown in Figure 9, CREAM TeV data [33] are in agreement with TIGER/HEAO-3 at lower energies. The data are consistent with the idea of GCR origin in OB associations, i.e., cosmic rays come from the core of super-bubbles, where OB associations enrich the interstellar medium with the outflow of massive stars (Wolf-Rayet phase and Supernovae). The data also imply preferential acceleration of elements found in interstellar grains compared with those found in interstellar gas, as well as mass-dependent acceleration [1].

4 Outlook

The CREAM-I results are based on ~ 13 days of live time out of ~ 26 days of stable data taking during its 42-day record-breaking flight. The first flight operations were not as efficient as later flights, but the ∼50% instrument dead time was caused mainly by communication errors from packet networking conflicts in the TCD system based on a TCP/IP protocol. The live time fraction increased to 75% for CREAM-II and 90% for CREAM-III and later flights. The live time was 99% when the TCD system was turned off during the CREAM-III and -IV flights due to a HV issue and during CREAM-V due to a TCD Ethernet switch failure.

One advantage of a balloon project is that the instrument can be improved each time it is flown. A redundant Science Flight Computer system was implemented for CREAM-III and subsequent flights to mitigate that potential single point failure in previous flights. Two computers were accommodated with a USB interface. Another improvement is a recoverable pallet. Using two halves of the CREAM-I and CREAM-II pallets, the CREAM-IV pallet was constructed using a piano hinge concept. This allows the recovered pallet to go through the Twin Otter door and be re-flyable through simple reassembly, as long as damage is not severe. The new quartet structure built for CREAM-III worked well to protect optical layers of the calorimeter during recovery, so only a fraction of them needs to be replaced. Nevertheless, each newly assembled calorimeter is calibrated at the European Organization for Nuclear Research (CERN) SPS, which provides the highest energy test beam particles available.

The same payload cannot be flown in consecutive years due to the time required for recovery, return to the laboratory, and refurbishment. Therefore, multiple copies of detectors were (or are being) constructed to take advantage of annual flight opportunities as they become available. The data from each flight reduces the statistical uncertainties and extends the measurement reach to energies higher than previously possible. Ultimately, CREAM will provide substantial overlap with and, thereby, calibration for ground-based, indirect measurements extending to much higher energies.

The unusually short flight of CREAM-VI was due to unplanned premature termination, the cause of which is unclear, although a balloon burst detector malfunction is suspected. The payload successfully parachuted to the ground. Although the payload was dragged ~ 400 m after impact, due to late parachute separation, the science instrument was recovered without any damage. The calorimeter, SCD and electronics boxes on the pallet were recovered as one piece without any disassembly, which marks the best recovery of the instrument requiring minimum repair. The recovered instrument came back from Antarctica in March 2011. The seventh flight will incorporate the refurbished calorimeter and double-layer SCD from the CREAM-VI flight, the same graphite targets, S3, and CD, a new TRD with improved tracking, and a TCD with improved electronics.

A USB-based TCD electronics readout scheme has been implemented to replace the current readout based on a TCP/IP protocol between 9 stacks of boards, each with an embedded microcontroller. While the earlier approach largely worked, it led to packet networking conflicts that resulted in communication errors and increased dead time (of up to ∼50%) that required the introduction of pre-scaling in the TCD triggering. In addition, a TCD Ethernet switch failed unaccountably during the CREAM-V flight.

One modification currently under consideration for future flights is an upgrade of the calorimeter readout boxes by providing a high voltage power supply (HVPS) for each two hybrid photo diodes (HPD's) instead of for each 5 HPD's. This modification would improve the "graceful degradation" of the calorimeter readout should HV problems occur in flight.

It should be noted NASA is currently developing a super-pressure balloon (SPB) capable of maintaining high-altitude with loads comparable to zero-pressure

balloons [2]. A 7 MCF SPB flew successfully for 54 days in Antarctica between December 2008 and February 2009, and a 14 MCF SPB completed its successful 22-day flight in January 2011. An 18 MCF SPB test flight is planned. The 26 MCF balloon is approximately the size still intended for the ULDB demonstration mission of 60 - 100 days with a 1,000 kg science instrument.

As ULDB becomes available, long-duration exposures can be achieved faster and more efficiently without multiple refurbishment and launch efforts. Whatever the flight duration (either LDB or ULDB), the data from each flight reduces the statistical uncertainties and extends the reach of measurements to energies higher than previously possible.

5 Acknowledgements

The authors thank the NASA Wallops Flight Facility, Columbia Scientific Balloon Facility, National Science Foundation Office of Polar Programs, and Raytheon Polar Services Company for the successful balloon launch, flight operations, and payload recovery for each balloon flight. This work is supported in the U.S. by NASA grants NNX11AC52G, NNX08AC15G, NNX08AC16G and their predecessor grants, as well as directed RTOP funds to the NASA Goddard Space Flight Center. It is supported in Korea by National Space Laboratory Program of National Research Foundation, and in France by IN2P3, CNRS, and CNES.

References

[1] E. S. Seo, 2012, Astropart. Phys., in press, http://dx.doi.org/10.1016/j.astropartphys.2012.04.002
[2] W. V. Jones, 2005, ICRC, 10, 173
[3] H. S. Ahn, et al., 2007, Nucl. Instr. Meth. Phys. Res. A, 579, 1034
[4] P. Maestro, et al., 2007, ICRC, 2, 333
[5] J. Chang, et al., 2008, Nature, 456, 362
[6] A. A. Abdo, et al., 2009, Phys. Rev. Lett., 102, 181101
[7] M. H. Lee, et al., 2008, IEEE T. Nucl. Sci., 56, 1396
[8] P. S. Marrocchesi, et al., 2008, Adv. Space Res., 41, 2002
[9] O. Bourrion, et al., 2011, J. Instr., 6, P06004
[10] H. S. Ahn, et al., 2009, Nucl. Instr. Meth. Phys. Res. A, 602, 525
[11] S. P. Wakely, et al., 2008, Adv. Space Res., 42, 403
[12] I. H. Park, et al., 2007, Nucl. Instr. Meth. Phys. Res. A, 570, 286
[13] S. Nam, et al., 2007, IEEE T. Nucl. Sci., 54, 1743
[14] A. Malinin, 2011, ICRC, 6, 411
[15] H. S. Ahn, et al., 2009, ApJ, 707, 593
[16] Y. S. Yoon, et al., 2011, ApJ, 728, 122
[17] O. Adriani, et al., 2011, Science, 332, 69
[18] H. S. Ahn, et al., 2010, ApJ, 714, L89
[19] O. Adriani, et al., 2009, Nature, 458, 607
[20] V. I. Zatsepin and N. V. Sokolskaya, 2006, A&A, 458, 1
[21] V. S. Ptuskin, et al., 2010, ApJ, 718, 31
[22] G. A. Medina-Tanco and R. Opher, 1993, ApJ, 411, 690
[23] F. Donato and P. D. Serpico, 2011, Phys. Rev. D., 83, 023014
[24] A. W. Strong, I. V. Moskalenko and V. S. Ptuskin, 2007, Annu. Rev. Nucl. Part. Sci., 57, 285
[25] C. J. Cesarsky, 1980, ARA&A, 18, 289
[26] H. S. Ahn, et al., 2008, Astropart. Phys., 30, 133
[27] J. J. Engelmann, et al., 1990, A&A, 233, 96
[28] D. Panov, et al., 2009, Bull. Rus. Acad. Sci. Phys., 73, 564
[29] A. Obermeier, 2011, PhD Thesis, Radboud Universiteit, Nijmegen, Germany
[30] E. S. Seo and V. S. Ptuskin, 1994, ApJ, 431, 705
[31] M. Casse and P. Goret, 1978, ApJ, 221, 703
[32] B. F. Rauch, et al., 2009, ApJ, 697, 2083
[33] H. S. Ahn, et al., 2010, ApJ, 715, 1400